Enzyme Adaptation to Inhibitor Binding: A Cryptic Binding Site in Phenylethanolamine *N*-Methyltransferase

Christine L. Gee,[†,‡,§] Nyssa Drinkwater,[†,‡] Joel D. A. Tyndall,[‖] Gary L. Grunewald,[⊥] Qian Wu,[#] Michael J. McLeish,[#] and Jennifer L. Martin*,[‡]

Institute for Molecular Bioscience and ARC Special Research Centre for Functional and Applied Genomics, University of Queensland, Brisbane, Qld, 4072 Australia, National School of Pharmacy, University of Otago, Dunedin, New Zealand, 9054, Department of Medicinal Chemistry, The University of Kansas, Lawrence, Kansas 66045-7582, and College of Pharmacy, University of Michigan, Ann Arbor, Michigan 48109

Received March 23, 2007

Shape complementarity is a fundamental principle of inhibitor design. Here we show that an enzyme for which the crystal structure has been determined (phenylethanolamine *N*-methyltransferase, PNMT) conceals a cryptic binding site. This site is revealed upon binding of inhibitors that are double the size of the physiological substrate. These large inhibitors are not predicted to bind in that they protrude through the accessible surface calculated from a PNMT/7-aminosulfonyl-1,2,3,4-tetrahydroisoquinoline (SK&F 29661) crystal structure, yet they are potent inhibitors of PNMT. We determined structures of the enzyme complexed with large inhibitors and found that the volume of the active site increases by 140 Å³ upon binding. Changes in active site size and shape are brought about by unfavorable side chain conformations and rigid body helix motions. The energetic cost is modest, estimated at 2−3 kcal/mol from mutational analyses. Our findings further underline the importance of protein flexibility in structure-based inhibitor design studies.

Introduction

Inhibition of phenylethanolamine *N*-methyltransferase (PN-MT[a]) is a means of blocking the production of epinephrine (adrenaline) in the central nervous system and thereby enabling the elucidation of the role of epinephrine as a neurotransmitter. Toward this end, we aim to develop inhibitors of human PNMT (hPNMT) that are potent and selective and that penetrate the blood−brain barrier.

The crystal structure of hPNMT has previously been determined in complex with the inhibitor, 7-aminosulfonyl-1,2,3,4-tetrahydroisoquinoline (SK&F 29661, **1**), and the cofactor product *S*-adenosyl-L-homocysteine (AdoHcy).[1] The structure revealed that **1** did not fully utilize the available space in the active-site cavity and suggested there was room for additional substituents at both the 3- and 7-positions (Figure 1) of the tetrahydroisoquinoline (THIQ) ring. A series of 3- and 7-sub-stituted THIQ inhibitors (Table 1) had previously been shown to have increased affinity for hPNMT compared with **1** (K_i value 120 nM, Table 1).[2] Surprisingly, THIQ inhibitors with 7-sub-stituents that are seemingly too large for the hPNMT binding pocket (**5**−**9**, Table 1) retained significant enzyme inhibitory

Figure 1. Accessible surface of the active site pocket of hPNMT with AdoHcy and SK&F 29661 (**1**) bound.[1] The 3- and 7-positions of the THIQ framework are indicated to show the additional space available in these regions of the active site. Hydrogens have been added to the structures of the ligands.

activity. For example, the PNMT inhibitor **8** has a *p*-chlorophe-nylsulfonamide substituent at the 7-position of the THIQ ring, yet racemic **8** inhibits hPNMT with a K_i value of 39 nM (Table 1). Clearly, if this ligand binds to the same hPNMT binding site as smaller 7-substituted THIQ compounds such as **1**, the binding pocket must adapt to accommodate the larger substitu-ent. Furthermore, these substituents must make interactions of sufficient strength to offset the energetic cost of these adapta-tions.

We investigated how hPNMT accommodates 7-substituted and 3,7-disubstituted THIQ inhibitors by using X-ray crystal-lography. The resulting crystal structures show that the enzyme adapts to the presence of large 7-substituents through side chain conformational changes, involving primarily Lys57, as well as

* To whom correspondence should be addressed. Institute for Molecular Bioscience, Queensland Bioscience Precinct, University of Queensland, 306 Carmody Road, Brisbane, QLD 4072 Australia. Phone: +61 7 3346 2016. Fax: +61 7 3346 2101. E-mail: j.martin@imb.uq.edu.au.
† Contributed equally to the work described in this manuscript.
‡ University of Queensland.
§ Present address: Department of Molecular and Cellular Biology, University of California Berkeley, Berkeley, CA 94720.
‖ University of Otago.
⊥ The University of Kansas.
University of Michigan.
[a] Abbreviations: PNMT, phenylethanolamine *N*-methyltransferase; hP-NMT, human PNMT; *wt*, wild-type; hPNMT$_A$, molecule A in the asym-metric unit of hPNMT crystals; hPNMT$_B$, molecule B in the asymmetric unit; AdoMet, *S*-adenosyl-L-methionine; AdoHcy, *S*-adenosyl-L-homocys-teine; THIQ, 1,2,3,4-tetrahydroisoquinoline. PDB: coordinates and structure factors for *wt* hPNMT complexed with **4**, **5**, **6**, and **7** and K57A hPNMT complexed with **5**, **7**, and **8** have been deposited with the protein data bank (2G70, 2ONY, 2G71, 2G72, 2ONZ, 2OBP, and 2OBF, respectively).
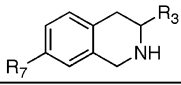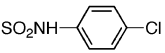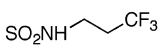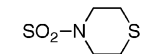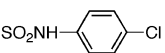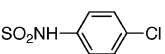
Table 1. Chemical Structures, Inhibition Constants (K_i, nM) and Calculated Free Energy (kcal/mol) Values of the Inhibitors for *wt* and K57A hPNMT[a]

	R_7	R_3	*wt* K_i	*wt* ΔG	K57A K_i	K57A ΔG	Fold change in K_i	$\Delta\Delta G$
1	SO_2NH_2	H	120 ± 20^b	−9.4	6900 ± 100^b	−7.0	0.02	−2.4
2	NO_2	H	78 ± 14^b	−9.7	1370 ± 5	−8.00	0.06	−1.7
3	I	H	40 ± 10^b	−10.1	740 ± 270^b	−8.4	0.05	−1.7
4	NO_2	$(+)CH_2OH$	17 ± 1	−10.6	145 ± 1	−9.3	0.12	−1.3
5	SO_2NH—〈 〉—Cl	H	210 ± 4	−9.1	1.3 ± 0.4	−12.1	162	+3.0
6	SO_2NH—CF_3	$(+)CH_2F$	35 ± 1	−10.2	17 ± 2	−10.6	2.1	+0.4
7	SO_2—N〈 〉S	$(+)CH_2F$	315 ± 29	−8.9	1.8 ± 1	−11.9	175	+3.0
8	SO_2NH—〈 〉—Cl	$(\pm)CH_2OH$	39 ± 1	−10.1	1.4 ± 0.1	−12.1	28	+2.0
9	SO_2NH—〈 〉—Cl	$(+)CH_2F$	46 ± 2	−10.0	1.0 ± 0.3	−12.3	46	+2.3

[a] K_i values are reported as ±standard error of the mean. Fold change in K_i refers to the ratio of K_i values for *wt* and K57A hPNMT. [b] Data from Wu et al.[6]

a rigid body movement of an active site helix by 0.5 Å or more and perturbation of a second active site helix. Together these changes increase the volume of the binding pocket by 140 Å³ at an energetic cost estimated from mutational analysis to be 2−3 kcal/mol.

Results

The crystal structures of *wt* hPNMT/AdoHcy with **5** or **6** and of *wt* hPNMT/AdoMet with **4** or **7** were solved at a resolution of 2.6, 2.2, 2.4, and 2.0 Å, respectively. We also solved the structures of K57A hPNMT/AdoHcy with **5**, **7**, or **8** at a resolution of 2.8, 2.8, and 2.3 Å, respectively. The statistics for the refined crystal structures are given in Table 2. The structure determination of hPNMT/AdoHcy/**8** is reported in detail elsewhere (pdb accession code 2G8N).[3] In brief, the diffraction data for the hPNMT/AdoHcy/**8** complex were measured to a resolution limit of 2.15 Å, and the structure was refined with *R*-factor and *R*-free values of 20.0 and 24.2%, respectively.

The crystal structures are isomorphous with previously published structures of hPNMT in complex with **1**, octopamine, 7-iodo-, or 7,8-dichloro-substituted THIQ.[1,4−6] The secondary structure and most of the tertiary structure of the enzyme in the structures of the complexes reported here are essentially identical to those described previously. The binding mode and contacts formed to the cofactor product AdoHcy are also consistent with those reported earlier,[1,4−6] and the AdoMet cofactor in the complexes with **4** and **7** is bound as predicted by modeling.[5]

7-*p*-Chlorophenyl Substituent Induces Disorder in Lys57. Inhibitor **5** has a bulky *p*-chlorophenyl substituent on the 7-sulfonamide group of the THIQ nucleus but no 3-substituent (Table 1). The addition of the *p*-chlorophenyl in the absence of a 3-substituent is unfavorable; thus, the K_i value for **5** is higher than that for **1** and much higher than that for **8** or **9**, which have the same 7-substituent in addition to a substituent at the

3-position (Table 1). The crystallization and crystal structure of hPNMT complexed with **5** supports this interpretation. Crystals of the hPNMT/**5** complex took 3−4 weeks to grow, in contrast to the 3−4 days needed for the other enzyme/inhibitor complexes to crystallize. Electron density corresponding to **5** was present in only one of the two molecules in the asymmetric unit and was poorly ordered for the *p*-chlorophenyl group (Figure 2B, Supporting Information, Figure 1). Furthermore, electron density was absent for much of the side chain of the critical active site residue Lys57, and these atoms were built with zero occupancy to indicate that their position is not defined. The poor density for Lys57 suggests that the *p*-chlorophenyl substituent induces disorder in this residue (Figure 2B). Lys57 was identified previously as important for substrate and inhibitor recognition,[1,5,6] and its flexible side chain was found to move within the active site to accommodate different inhibitor substituents.[4] In previously determined structures, the Lys57 side chain amine interacts with a water or an inhibitor sulfonamide.[1,4] The disordered nature of Lys57 in the crystal structure of hPNMT complexed with **5** is probably a consequence of the lack of a binding partner for this buried charged residue.

Major Perturbations of the Active Site to Accommodate 3,7-Disubstituted THIQs. Inhibitor **8** has the same chemical structure as **5** but with the addition of a 3-hydroxymethyl substituent (Table 1). The combination of the *p*-chlorophenyl group, and the 3-substituent in **8** is favorable for binding to hPNMT. Thus, the K_i value for racemic **8** is lower than that for **5** (which lacks the 3-substituent) and also lower than that for **1** (which lacks both the 3-substituent and the *p*-chlorophenyl moiety; Table 1). Unlike that for **5**, the electron density for **8** is well-ordered.[3] The structure reveals significant changes for the side chain conformations of Lys57 and Cys60 (Figures 2C and 3G). Lys57 adopts a conformation very different to that observed previously (Figure 3G compared with 3A,B). The probability

Table 2. Statistics for hPNMT Crystallographic Data Measurement and Structure Refinement

inhibitor/cofactor protein	(R)-**4**/AdoMet *wt* hPNMT	**5**/AdoHcy *wt* hPNMT	**5**/AdoHcy K57A hPNMT	(R)-**6**/AdoHcy *wt* hPNMT	(R)-**7**/AdoMet *wt* hPNMT	(R)-**7**/AdoHcy K57A hPNMT	(R)-**8**/AdoHcy K57A hPNMT
space group	$P4_32_12$	$P4_32_12$	$P4_32_12$	$P4_32_12$	$P4_32_12$	$P4_32_12$	$P4_32_12$
Unit Cell							
a,b (Å)	94.2	94.0	94.5	94.2	94.3	94.4	94.7
c (Å)	187.8	188.0	187.9	188.2	188.9	187.7	188.3
α,β,γ (°)	90	90	90	90	90	90	90
No. observations	237 112	164 639	100 484	328 818	681 279	170 045	128 948
No. unique	33 540	26 667	21 552	43 750	58 197	24 041	38 682
resolution (Å)	29.80−2.40	45.58−2.6	54.45−2.80	34.96−2.20	32.84−2.00	66.77−2.80	34.00−2.30
(top shell)	(2.49−2.40)	(2.69−2.60)	(2.90−2.80)	(2.28−2.20)	(2.07−2.00)	(2.90−2.80)	(2.38−2.30)
redundancy	7.07 (7.25)	6.17 (6.20)	4.66 (4.68)	7.52 (7.53)	11.71 (11.38)	7.06 (7.25)	3.33 (3.32)
$I/\sigma I$	12.7 (3.6)	14.3 (2.2)	10.4 (2.1)	14.3 (4.6)	17.5 (4.6)	7.7 (2.0)	11.1 (2.0)
completeness[a] (%)	99.0 (97.9)	99.9 (100.0)	99.3 (99.9)	99.9 (100.0)	99.8 (99.0)	99.8 (100.0)	99.6 (100.0)
R_{merge}[b] (%)	7.4 (55.9)	5.1 (49.5)	7.6 (51.4)	6.5 (42.0)	5.9 (55.7)	11.4 (52.8)	4.9 (49.4)
Refinement							
No. reflections (|F| > 0)	33 484	26 704	21 710	43 749	58 130	21 653	38 856
total (test set)	(3339)	(1220)	(1009)	(4401)	(5908)	(1034)	(1863)
R_{cryst}[c]/R_{free}[d] (%)	24.0/28.5	22.3/25.8	21.7/26.3	21.3/25.1	22.6/26.2	23.6/27.7	21.7/26.7
(top shell)	(41.5/43.5)	(43.1/37.8)	(35.7/38.9)	(32.9/33.8)	(45.7/45.8)	(36.6/38.8)	(35.6/35.6)
No. nonhydrogen atoms	4299	4337	4311	4524	4564	4245	4492
protein	4123	4101	4093	4146	4208	4093	4120
cofactor	50	52	52	52	54	52	52
inhibitor	42	21	42	44	42	42	46
water	79	158	105	276	260	73	274
other	5 (phosphate)	5 (phosphate)		6 (glycerol)		5 (phosphate)	
RMSD from Ideal Geometry							
bond length (Å)	0.008	0.007	0.007	0.006	0.008	0.008	0.007
bond angle (deg)	1.4	1.3	1.3	1.3	1.4	1.5	1.3
Average B-Factor (Å^2)							
all	60.3	68.8	64.4	48.1	48.0	76.2	58.2
protein	60.1	68.7	64.8	47.6	47.7	76.6	57.8
cofactor	70.2	64.6	57.0	42.6	48.9	68.9	50.4
inhibitor	71.4	77.6	56.6	73.5	39.1	66.8	45.1
water	54.4	65.8	56.7	52.8	52.1	64.1	60.9
other	158.7	99.7		73.7		138.4	
Luzzati Coordinate							
error (Å)	0.37	0.39	0.39	0.29	0.30	0.44	0.34
cross-validated error (Å)	(0.46)	(0.47)	(0.45)	(0.34)	(0.35)	(0.55)	(0.41)
Ramachandran Plot							
% in most favored region	88.3	90.8	90.3	91.8	93.6	89.0	91.5
% in disallowed region	0.0	0.0	0.0	0.0	0.0	0.0	0.0

of the new conformation is low, estimated at 0.05%,[7] compared with ∼4% for the previously reported rotamer of Lys57 in hPNMT. In the new conformation, the side chain of Lys57 interacts with one of two alternate conformations modeled for the side chain of Cys60 (Figures 2C and 3G). The conformation of the side chain of Cys60 that interacts with Lys57 is also altered compared with those observed in previous structures (Figure 3G compared with 3A,B). The new conformation of the Cys60 side chain, with a χ_1 value of 116°, is neither in an extended (180°) nor gauche (−) (60°) conformation, but is instead oriented in an unfavorable or low probability conformation of close to 120°. In contrast, the previously observed conformation for the Cys60 side chain has a χ_1 value of −65°, close to ideal for a low-energy gauche (+) rotamer. The probability for this previously observed conformation is 57%.[7]

In addition to the side chain conformational changes, there is a rigid body displacement of 0.5−0.7 Å by the part of the active site helix α3 that incorporates Lys57 and Cys60 (Figure 3I) in comparison to the structures complexed with inhibitors **1**, **2**, and **3** that have much smaller 7-substituents. There is also a perturbation of the first turn of helix α4 and a rotation of the side chain of Tyr126 (located on the α4 helix) away from the active site (Figure 3J) upon binding **8**. The Tyr126 side chain, which forms a water-mediated interaction with the Arg44 mainchain oxygen in the hPNMT/**1** complex (Figure 3A), instead forms a hydrogen bond to the mainchain oxygen of Tyr40 in the complex with **8** (not shown).

These same perturbations to Lys57, Cys60, Tyr126, α3, and α4 are also observed in hPNMT upon binding **7** (Figure 3F,I,J). This inhibitor, like **8**, has both a 3-substituent and a bulky substituent on the 7-sulfonamide THIQ framework. Conversely, when a flexible aliphatic chain is substituted in this position, as in **6**, or the 3-substituent is lacking, as in **5**, we only observe the changes to Tyr126 and α4 (Figure 3I,J), suggesting that it is the combination of the 3-substituent and the bulky 7-substituent that induces the major conformational effects in hPNMT.

However, to rule out any direct effect of the 3-substituent in causing the conformational changes at α3, we determined the structure of hPNMT in complex with **4**. This inhibitor has a small 7-nitro substituent on the THIQ nucleus, like that of **2**, and in addition has a 3-hydroxymethyl substituent, like that of **8**. As expected, the enzyme in the structure with **4** had none of the perturbations described above for Lys57, Cys60, Tyr126, α3, or α4. This confirms that a combination of a bulky 7-substituent and a 3-substituent is required to induce the changes in the enzyme active site architecture.

Collectively, the side chain and mainchain movements described above increase the volume of the inhibitor binding
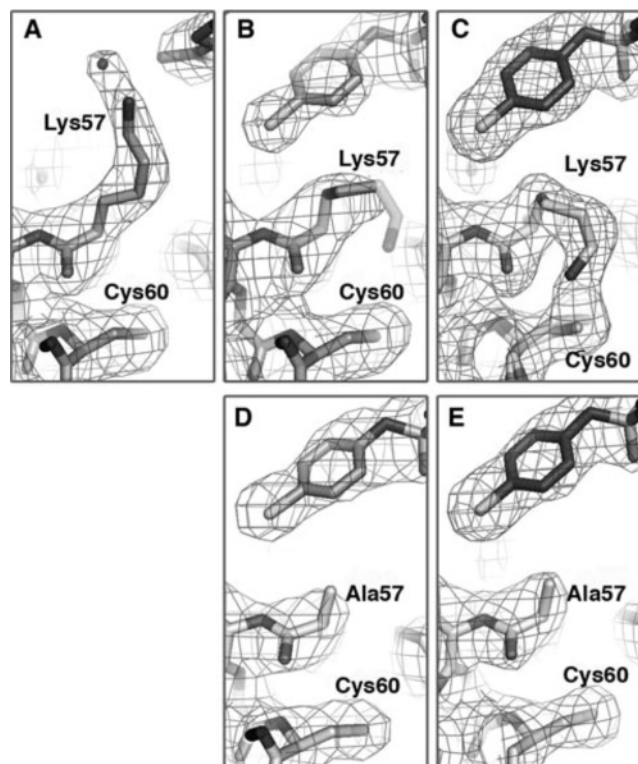
Figure 2. Omit electron density contoured at 3σ in the region around residues Lys57 and Cys60. **A**, **B**, and **C** show inhibitors **4**, **5**, and **8** bound to *wt* hPNMT, and **D** and **E** show **5** and **8** bound to K57A PNMT. The transparent atoms of the Lys57 side chain in **B** indicate zero occupancy and a lack of a defined position. The 7-substituent of each inhibitor is shown at the top right of each figure.

pocket compared with the originally described hPNMT structures (from $\sim$450 Å^3 for **1** to $\sim$520 Å^3 for **6** and $\sim$590 Å^3 for **7** and **8**, Figure 4). This increase in volume is apparently due to the changes that occur at Lys57. In the K57A mutant structures with **5**, **7**, and **8** bound (see below), the volume of the active site is calculated to be $\sim$610 Å^3 (Figure 4D).

Effect of 3- and 7-Substituents on Inhibitor Binding. Superimposition of the bound conformations of inhibitors **4**−**8** with that of **1** (representing the simplest inhibitor) allows comparison of their binding position and orientation within the enzyme active site. All four compounds that have 3-substituents (**4**, **6**, **7**, and **8**) are rotated by 10−15° about the long axis of the THIQ framework compared with **1**, to allow optimal binding interactions of the 3-substituent (Figure 5A,C,D). This rotation is not observed for **5**, which lacks a 3-substituent (Figure 5B). Instead, **5** is translated in the binding site by 0.5−0.6 Å in the direction of the THIQ 3-position compared with **1**, presumably to enable the binding of the bulky 7-substituent in the sterically restricted binding site. Notably, the distance that **5** is translated in the active site (to the right in Figure 5) is the same magnitude as the rigid body movement of α3 (to the left in Figure 5) when **7** or **8** are bound. We surmise that the bulky 7-substituents of **5**, **7**, and **8** require additional binding volume at the active site compared with **1**. An increase in binding volume is achieved rather inadequately for **5** (given the poor binding of this inhibitor) by the 0.5−0.6 Å shift of the inhibitor in the active site. The presence of a 3-substituent in **7** and **8** prevents such a shift because of the additional steric bulk. Instead, it is the enzyme that adapts to increase the binding volume for the 7-substituent. It does so by the rigid body motion of helix α3 and by side chain conformational changes to Lys57 and Cys60.

Molecular Basis for the Binding Potency of 7-Sulfonamide Substituents. In the enlarged active site of hPNMT, favorable interactions that were not possible in the previously described structures are observed to occur between the enzyme and the bulky 7-substitutents of **7** and **8**. The aromatic substituent of **8** forms edge−face interactions with the side chain of Tyr40 and the *p*-chloro group fits into a hydrophobic pocket formed by the sidechains of Leu58, Tyr85, Tyr126, and Gly54 and the aliphatic chain of Lys57. This binding interaction provides the molecular basis for the observation that a *p*-substituent, but not a *m*-substituent, increases the activity of this series of inhibitors.[8] In the structure of hPNMT complexed with **1**, Lys57 interacts with the sulfonamide of the inhibitor (Figure 3A). However, when **8** is bound and Lys57 adopts a new conformation, the sulfonamide rotates so that it is within the hydrogen bond distance of the Asn39 mainchain oxygen (Figure 3G). This interaction contributes significantly to inhibitor binding, because replacement of the sulfonamide with a sulfone reduces binding potency.[3]

The *p*-chlorophenyl of **5** is similarly placed to that of **8** (Figure 5D) though the disordered electron density of the *p*-chlorophenyl suggests weaker binding for **5**. This is confirmed by B-factor analysis of **5** and **8**. In the structure of hPNMT/**8**, the average B-factor for the inhibitor (42 Å^2) is lower than the value for all protein atoms (51 Å^2), suggesting that it is tightly bound and well-ordered. In contrast, the average B-factor for **5** is higher (78 Å^2) than that for protein atoms (69 Å^2), indicating that it is bound more weakly and poorly ordered. However, when Lys57 is mutated to Ala in the K57A hPNMT structures, the B-values for **5** (57 Å^2) are lower than for protein (65 Å^2), as is the case for **8** (45 Å^2 and 58 Å^2, respectively, for inhibitor and protein B values). This suggests that it is the interplay between Lys57 and **5** that induces the disorder observed in both.

The aliphatic thiomorpholino group of **7** interacts with the same residues as the *p*-chlorophenyl group of **8**. However, the lack of aromatic resonance likely makes the edge−face interaction less favorable, possibly contributing to the lower binding affinity of **7** in comparison with **8** (Table 1). Inclusion of sulfur in this aliphatic ring increases inhibitory potency by a factor of 4 compared with a carbon ring system.[8] This is likely due to the stronger interaction of sulfur with the mainchain Cα of Gly54 and the ring edges of Tyr40 and Tyr126. The 7-substituent of **6** forms interactions similar to those for **7** and **8**. In addition, the Tyr126 side chain hydroxyl is within hydrogen bond distance (2.9−3.1 Å) of a fluorine of the 7-trifluoropropyl group of **6**. Though such an interaction may be weak, there is evidence from other protein−ligand crystal structures that they do occur.[9]

An Estimate of the Energetic Cost of the Active Site Perturbations. The changes in the hPNMT active site upon binding **7** or **8** are due in large part to the presence of the highly flexible side chain of Lys57 in the active site. To make room for the large 7-substituents, the side chain of Lys57 adopts an unfavorable rotamer conformation and induces an unfavorable conformation in the side chain of Cys60. In addition, there is a rigid body movement of the α3 helix on which these residues are located. We evaluated the effect of these conformational changes using the hPNMT mutant K57A, which we had prepared previously to investigate the role of this side chain on the binding of **1**, **2**, and **3**.[6] For the THIQ derivatives with small 7-substituents, the mutation of Lys57 significantly *reduces* binding affinity (by 8−50-fold or 1.3−2.4 kcal/mol) of these three inhibitors and of inhibitor **4** (which also has a 3-substituent). This result is likely due to the loss of a favorable hydrogen
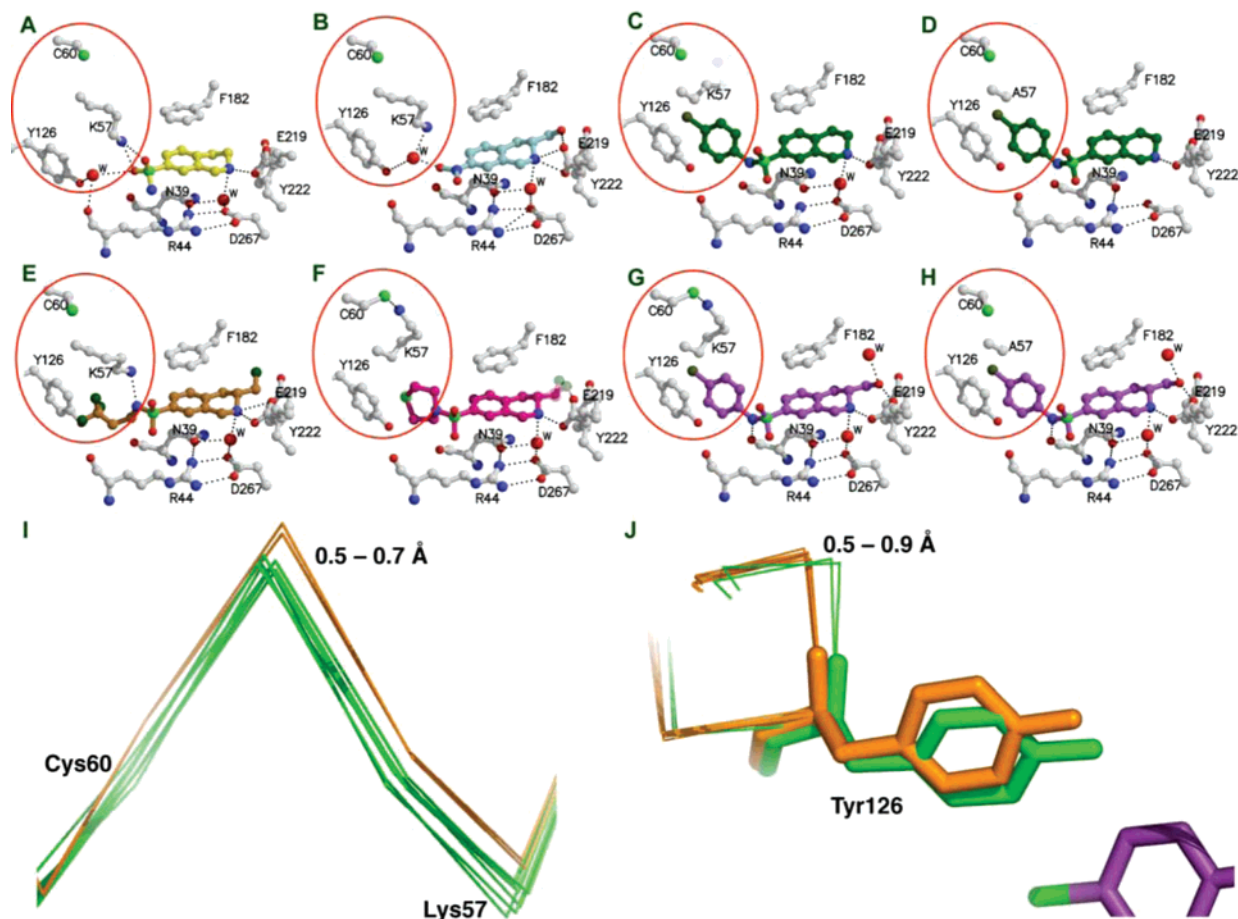
Figure 3. Enzyme−inhibitor interactions at the hPNMT active site with THIQ inhibitors bound. The sidechains of residues that move significantly upon binding **7** and **8** (Lys57, Cys60, and Tyr126) or that are mutated (K57A) are circled in red. hPNMT/inhibitor complexes shown are **A**, *wt* hPNMT/**1** (yellow); **B**, *wt* hPNMT/**4** (blue); **C**, *wt* hPNMT/**5** (green); **D**, K57A hPNMT/**5** (green); **E**, *wt* hPNMT/**6** (orange); **F**, *wt* hPNMT/**7** (pink), showing the two alternate conformations of the 3-fluoromethyl substituent; **G**, *wt* hPNMT/**8** (purple); and **H**, K57A hPNMT/**8** (purple). (**I**) Rigid body movement of the α3 helix. Helices from the *wt* hPNMT complexes with **7** and **8** are colored orange (the perturbed structure) and all others (*wt* hPNMT **1**, **4**, or **6** and K57A hPNMT with **7** or **8**) are colored green (the unperturbed structure). The position of Lys57 and Cys60 are indicated. (**J**) The α4 helix and Tyr126 in *wt* and K57A hPNMT structures. The first turn of helix α4 and the conformation of Tyr126 are shown. Cα traces of *wt* hPNMT with **1** and **4** are colored green (the unperturbed structure) and those of *wt* hPNMT with **5**, **6**, **7**, and **8** and K57A hPNMT with **5**, **7**, and **8** are colored orange (the perturbed structure). The conformation of Tyr126 from the structure of hPNMT complexed with **1** is shown in green (unperturbed), while that of **8** is shown in orange (perturbed). The bound position of the 7-*p*-chlorophenyl substituent of **8** is shown for reference (green/purple).

bond and a decrease in entropy due to the need to fill the space with water molecules. By comparison, the K57A mutation significantly *increases* the binding affinity of **7** and **8** (by 28−175-fold or 2−3 kcal/mol), the two inhibitors that cause major active site perturbations.

Binding of **5** induces disorder in the Lys57 side chain rather than an unfavorable conformation. It is interesting that mutation of Lys57 to alanine significantly *increases* the binding affinity of **5** (by 160-fold or 3 kcal/mol). This outcome suggests that the disordered state of Lys57, and the consequent lack of a hydrogen bond partner for this buried charged residue, is energetically costly.

We also examined the hPNMT inhibition of **9**, which is structurally related to **8**, in that both possess the same 7-*p*-chlorophenylsulfonamide substituent on the THIQ nucleus. The difference between the two compounds is that **9** contains a 3-fluoromethyl substituent, whereas **8** has a 3-hydroxymethyl substituent. In the absence of a crystal structure of hPNMT complexed with **9**, we predicted that **9** would cause similar active site conformational changes to those induced by the binding of **7** or **8**. This prediction was broadly borne out as the data for **9** (Table 1) show that it binds the K57A mutant almost

50-fold (or 2.3 kcal/mol) more tightly than the *wt* enzyme. Notably, the inhibition of hPNMT by **6**, which does not induce changes to Lys57 or the α3 helix, but does perturb the α4 helix, is also improved by mutation of Lys57. However, in this case, the improvement is just 2-fold (0.4 kcal/mol).

Effect of K57A Mutation on Inhibitor Binding and Protein Structure. The considerable changes we observe in the binding volume of hPNMT appear to stem largely from the interplay between Lys57 and bulky 7-substituents of the inhibitors. We therefore determined the crystal structures of K57A hPNMT in complex with the inhibitors **5**, **7**, and **8**. In all three complexes, the inhibitor binding position is similar to that of *wt* hPNMT. Both the K_i values (Table 1) and B-factor analysis of **5**, above, indicate tighter inhibitor binding for K57A than with *wt* hPNMT, and the fact that the K57A hPNMT/**5** crystals grow easily within 2−3 days supports a stronger interaction. Collectively, these results agree with a scenario in which an unfavorable interaction occurs between the *p*-chlorophenyl of **5** and the side chain of Lys57 in the *wt* hPNMT/**5** complex. It is this interaction that is responsible for the disorder observed in the crystal structure
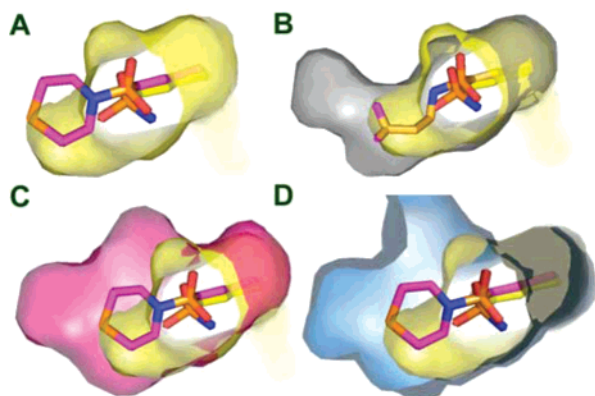
Figure 4. Volume changes at the active site of hPNMT (**A**) The solvent accessible surface of the hPNMT active site pocket near the 7-position of THIQ from the crystal structure of hPNMT in complex with **1** (yellow) shows that **7** (pink) protrudes through the surface (volume 450 Å³). (**B**) The accessible surface at the active site based on the crystal structure of hPNMT in complex with **6** (gray) overlaid with the accessible surface determined for the complex with **1** (yellow), showing the increased volume in the active site (510 Å³). (**C**) The accessible surface at the active site based on the crystal structure of hPNMT in complex with **7** (pink) overlaid with the solvent accessible surface determined for the complex with **1** (yellow), showing the increased volume of the active site (∼590 Å³). (**D**) The accessible surface at the active site based on the crystal structure of K57A hPNMT in complex with **7** (blue), showing that mutation of Lys57 to alanine creates a similar sized binding pocket (∼610 Å³) to that induced by the unfavorable conformational changes observed for Lys57.

and the reduced binding affinity of the inhibitor. Mutation of Lys57 to Ala relieves the strain, allowing a tighter binding interaction.

The K57A hPNMT structures complexed with **7** and **8** do not exhibit the rigid body displacement of the α3 helix that was observed in the *wt* hPNMT structures (Figure 3I). Because these changes are not observed in the K57A hPNMT structures, it seems likely that they are induced by the interaction between Lys57 and these large inhibitors. However, it is noteworthy that in all three crystal structures of K57A hPNMT, with **5**, **7**, and **8**, the perturbations observed for α4 and Tyr126 are present. This suggests that the α4 changes may be caused by steric interaction between the inhibitors and Tyr126.

Interactions Formed by the THIQ 3-Substituent. The crystal structures reported here allow us to investigate the relative binding of 3-hydroxymethyl (**4**, **8**) and 3-fluoromethyl (**6**, **7**) groups (Figure 3). The 3-hydroxymethyl forms a favorable hydrogen bond via a direct interaction with the side chain of Glu219 (as predicted by modeling studies;[10] Figure 3B,G,H) and possible water-mediated interactions with the side chain of Glu185 and mainchain oxygen of Phe182 (not shown).

We found that the bound conformation of the 3-fluoromethyl substituents is variable. For example, the 3-fluoromethyl of **7** adopts different orientations in the two molecules in the asymmetric unit (Figure 3F). In one of the two (modeled in hPNMT_A), the fluorine is located close to the bound position of the 3-hydroxyl group of **8** or **4**. In this orientation, the fluorine is within the hydrogen bond distance of the acidic side chain of Glu219. However, such an interaction would only be favorable if the Glu219 side chain is protonated, because fluorine is a hydrogen bond acceptor. In the second orientation (hPN-MT_B), the fluorine is within the hydrophobic interaction distance of the donor methyl group of AdoMet and within the hydrogen bond distance of a water (not shown). In both orientations, the fluorine is within hydrophobic interaction distance of Tyr222
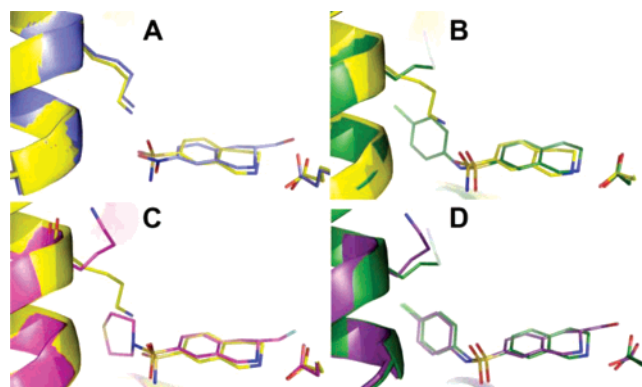
Figure 5. Comparison of the binding modes of THIQ inhibitors. The superimposed bound inhibitors are shown with helix α3, including Lys57 on the left and residue Glu219 on the right. (**A**) Compared with **1** (yellow), the addition of a 3-substituent in **4** (blue) induces a rotation around the long axis of the THIQ nucleus to enable access of the 3-substituent to the accessory binding cavity. A similar rotation is observed in other THIQ inhibitors with a 3-substituent (panel C). (**B**) Compared with **1** (yellow), the addition of a large bulky 7-substituent in **5** (green) causes a translational shift (to the right in this orientation) to enable the 7-substituent to fit within the steric constraints of the binding site. This shift is also apparent in panel **D**. The 7-substituent induces a disordered conformation of the Lys57 side chain, represented by transparent atoms. (**C**) Comparison of **1** (yellow) and **7** (pink). Inhibitors **7** (pink) and **6** and **8** (not shown), which have substituents at both 3- and 7-positions, do not undergo the translation observed upon binding **5**, but do undergo the rotation observed for **4** (shown in panel A). (**D**) Inhibitors **5** (green) and **8** (purple) both have large, bulky 7-substituents. Compound **5** is translated in the active site (to the right in this orientation) so that the bulky 7-substituent can fit (inducing a disordered conformation of the Lys57 side chain, represented by transparent atoms). Inhibitor **8** (and **7**, not shown) cannot undergo this shift because of the steric effect of the 3-substituent. Instead, conformational changes are induced in the enzyme, centered around Lys57, which increases the volume of the binding site.

(3.5−3.6 Å). The second conformation is similar to that predicted by modeling studies.[10] In the structure of hPNMT with **6**, the electron density for the 3-fluoromethyl group is weak or absent, suggesting that for this compound the fluorine does not form significant interactions with the enzyme. The varying position of the 3-fluoromethyl group indicates that it does not form especially favorable interactions. This finding agrees with comparisons of 3-methyl and 3-fluoromethyl THIQ inhibitors, showing that these have similar activities and indicating that the fluoro group does not contribute much toward binding affinity.[11]

Discussion

Our results show that the binding site of hPNMT is plastic. It is able to accommodate small substrates such as norepinephrine as well as fused ring inhibitors such as THIQ and much larger substituted THIQ derivatives. This plasticity is, in the main, due to the flexibility of the side chain of the active site residue Lys57 as well as perturbations of secondary structural elements in the active site. The crystal structures of hPNMT complexed with **7** or **8**, THIQ derivatives with large 7-thiomorpholinosulfonyl and 7-*N*-(*p*-chlorophenyl)aminosulfonyl groups, respectively, reveal a considerable increase in the volume of the hPNMT binding pocket of ∼140 Å³. The volume increase of the active site cavity is brought about by an unfavorable conformation of the side chain of Lys57, an induced unfavorable conformation of the Cys60 side chain, as well as rigid-body helix perturbations. These changes in the active site allow these two large compounds to bind with high affinity to hPNMT.

Structural characterization of the complexes of K57A hPNMT with **5**, **7**, and **8** revealed no perturbation to Cys60 or to the active site helix α3, indicating that these changes observed in *wt* hPNMT are a direct result of interactions with the conformationally flexible Lys57. The key role played by Lys57 allowed us to estimate the energetic cost of the changes by analyzing the binding affinity of inhibitors to *wt* and K57A hPNMT. The binding affinity of THIQ inhibitors with small 7-substituents (**1**, **2**, **3**, and **4**) were reduced by 8−50-fold (1.3−2.4 kcal/mol) for the K57A mutant due to the loss of a favorable interaction with the Lys57 side chain. In contrast, the binding affinity of THIQ inhibitors with large, bulky 7-substituents was significantly improved for the K57A mutant compared with *wt* by 30−175-fold (∼2.0−3.0 kcal/mol). Similarly, the affinity of **5** for K57A hPNMT is increased by 160-fold (3.0 kcal/mol) compared with *wt*. This change indicates that the disordered nature of the Lys57 side chain and the *p*-chlorophenyl substituent of **5** are energetically costly, presumably because of the buried unpaired charge of the Lys57 side chain.

Lys57 clearly plays a critical role in ligand binding in PNMT; it contributes to binding affinity for ligands with small hydrophilic 7-substituents by donating hydrogen bonds, it contributes to binding affinity for ligands with small hydrophobic 7-substituents by subtle conformational changes that allow interaction of the substituent with Met258[4] and it affects binding affinity for ligands with large 7-substituents by adopting either a disordered conformation or a low probability conformation that induces other structural perturbations at the active site. Lysines are known to be particularly flexible acceptors in interactions involving ligands.[12] The importance of Lys57 for PNMT activity is further highlighted by the fact that it is conserved in the sequences of all known mammalian full-length PNMT enzymes (human (NP_002677.1), chimp (XP_511459), rhesus monkey (XP_001089850), cow (NP_803471.1), pig (ABI97171), mouse (1903270A), rat (CAA53082.1), dog (XP_548143.2), and opossum (ENSEMBL GENSCAN00000038194)). Indeed, the entire sequence motif 52-GVGPW**K**LR**C**-60 is conserved in the mammalian PNMT orthologues (∼75−90% sequence identity with hPNMT) and both Lys57 and Cys60 are conserved in pufferfish (ENSEMBL GENSCANSLICE00000024452) and zebrafish (XP_700125.1) PNMT sequences (45−50% identity).

The conformational changes we observed in hPNMT are not easily predicted in that the Lys57 and Cys60 conformations are low probability and are accompanied by rigid body helix movements. It is somewhat surprising then that these changes that increase the binding site volume can occur at such a relatively small energetic cost. This cost could reasonably be expected to be accommodated by most enzyme/protein systems. There are, of course, many examples in the literature of protein flexibility, as reviewed recently by Teague.[13] However, most examples compare bound versus unbound protein conformations or reveal relatively minor changes in side chain conformations. A cryptic binding site was uncovered in p38 MAP kinase upon binding a modified inhibitor,[14] but in that instance the energetic cost was not evaluated.

Could the conformation of Lys57 be modeled using rotameric sampling? We performed a docking study for inhibitors **1**, **7**, and **8** in which the side chains of the three hPNMT residues identified to be flexible (Lys57, Cys60, Tyr126) were allowed freedom to rotate during the docking calculations. The binding mode of **1** was predicted using this approach, but the binding modes of **7** and **8** were not (data not shown). Relative to the observed binding mode, both **7** and **8** were translated in the direction of the THIQ 3-position and rotated along the THIQ

axis, and unfavorable steric interactions were formed with the sulfonamide oxygen, the THIQ ring, and the *p*-chloro group. The conformation observed for the Lys57 side chain in the crystal structure (a high-energy *syn*-pentane-like conformation) is also not predicted using this approach. Instead, a conformation is predicted (rotamer probability 2.4%) that makes unfavorable steric interactions with the nearby Tyr185. We speculate that the observed high energy conformations of Lys57 and Cys60 in the hPNMT/**7** and hPNMT/**8** complexes may be stabilized by a buried amine-thiolate charge−charge interaction that is induced when the two sidechains are in close proximity. This would help explain the difficulty in predicting the observed conformational changes.

In summary, hPNMT conceals a cryptic binding site that is uncovered through unexpected conformational changes when large inhibitors are bound. This cryptic binding site is likely to be present in all mammalian PNMTs because the residues involved in the conformational changes are conserved in the known sequences of mammalian PNMTs.

Experimental Section

Crystallization of hPNMT. C-terminally His$_6$-tagged *wt* hPNMT was expressed and purified as described previously.[5,8] C-terminally His$_6$-tagged K57A mutant hPNMT was expressed and purified in the same way. Protein was concentrated to 50−60 mg/mL and mixed with inhibitor (final concentration 9−40 mM) and substrate *S*-adenosyl-L-methionone (AdoMet, final concentration 2 mM) or product *S*-adenosyl-L-homocysteine (AdoHcy, final concentration 1.7−3.6 mM), taking the final concentration of protein to 35−44 mg/mL or 1−1.2 mM. The protein mixture was crystallized by hanging drop vapor diffusion using drops comprising of 1 or 2 μL of protein and 1 or 2 μL of precipitant equilibrated over 100 or 400 μL of precipitant solution (0.6−1.2 M ammonium phosphate, 0.1 M sodium citrate pH 5.3−5.8 for inhibitor **4**, and 5−8% polyethylene glycol average molecular weight 6 K, 0.25 M LiCl, 0.1 M Na cacodylate pH 5.4−6.0 for all other inhibitors). Crystals of hPNMT with **5** required seeding and took 3−4 weeks to grow, whereas other crystals appeared within 2−3 days. The *R*-enantiomers of **4**, **6**, and **7** were used for the crystallization experiments. Racemic **8** was used in crystallizations, but only the *R*-enantiomer was bound to the enzyme. Phosphate buffer was used for the immobilized metal affinity chromatography purification of hPNMT and, in some cases (**5** with *wt* hPNMT, **7** with K57A hPNMT), phosphate copurifies and cocrystallizes with the protein even though phosphate was not included in the crystallization buffer.

Data Collection. Crystals of dimensions ∼0.25 × 0.25 × 0.25 mm^3 were cryoprotected either by dipping into mother liquor supplemented with 25% glycerol for 30 s to 2 min or by stepping through mother liquor supplemented with 10, 20, and then 30% ethylene glycol for 1−2 min each. In both cases, crystals were then flash-cooled in a nitrogen gas stream at 100 K. X-ray diffraction data were measured using a Rigaku FR-E copper rotating anode generator operating at 45 kV, 45 mA with Osmic Confocal Max-Flux optics (either HiRes[2] or Maxscreen). Reflections were measured with an R-AXIS IV^{++} imaging plate area detector. A Cryo Industries CryoCool LN2 was used for cooling the crystals during data measurement. Data were processed using Crystal Clear (Rigaku Corporation, (c) 1997−2002) and phasing was carried out using CNS v1.1.[15]

Structure Determination. The structures were solved by difference Fourier methods using the structure of PNMT/AdoHcy/**1** (PDB accession code 1HNN[1]) as the starting model. The asymmetric unit was chosen so that the disulfide bonds observed in the structure were formed between molecules in the same asymmetric unit. Model building was performed using O[16] or COOT[17] and the structures were refined using CNS v1.1[15] or REFMAC[18] followed by refinement in CNS. Initial coordinates for the inhibitors were generated using the Insight II 2000.1 (Accelrys) builder module or

SYBYL 7.0 (Tripos Associates Inc., 1699 S Hanley Rd., St. Louis, MO 63144). Topology and parameter files were generated using PRODRG[19] or XPLO2D[20] and modified where necessary. The procedure used was to refine the structure of the protein first, then water molecules were added, followed by addition of AdoHcy (or AdoMet), and finally the inhibitor was added. The criteria for including a water molecule were the presence of $2F_o - F_c$ density at 1σ and $F_o - F_c$ density at 3σ and a possible hydrogen bond with a distance of less than 3.5 Å. *R*-free analysis (10% of reflections for **4**, **6**, and **7** with *wt* hPNMT or 5% of reflections for **5** with *wt* and **5**, **7**, and **8** with K57A hPNMT) was used for cross-validation.[21] Electron density for inhibitors **4**, **6**, **7**, and **8** was clear and unambiguous in both molecules (hPNMT$_A$ and hPNMT$_B$) in the asymmetric unit of *wt* and K57A hPNMT. This was also the case for **5** bound to K57A hPNMT. However, for the complex of *wt* hPNMT and **5**, electron density corresponding to the inhibitor was only present in hPNMT$_A$; at the hPNMT$_B$ active site, the electron density was consistent with a bound phosphate ion that copurifies with the protein. Consequently, analyses of **5** bound to *wt* hPNMT refer to hPNMT$_A$. The electron density for the inhibitors was consistent in each case with the 3*R*-enantiomer. A figure showing the OMIT electron density for the inhibitors in all seven structures reported here is provided as Supporting Information Figure 1.

For structural analysis, hPNMT structures were superimposed by Cα position using COOT or the lsq module in O. Distances between equivalent Cα atoms of the overlaid structures were then measured. Procheck[22] was used to analyze the geometry and COOT was used to analyze rotamer probabilities, based on frequency of appearance in the PDB.[7] The program CASTp[23] with default settings was used to calculate the cavity volumes. The likelihood of virtual screening programs identifying compounds such as **7** and **8** as hits was evaluated by docking these inhibitors, and inhibitor **1**, into the PNMT active site. GOLD v3.1 (copyright 2004, the Cambridge Crystallographic Data Centre) was used for the docking calculations. Three active site residues were identified as flexible (Lys57, Cys60, and Tyr126), and these were allowed to undergo torsional rotation around acyclic side chain bonds based on rotamer libraries;[24] the inhibitors were allowed full flexibility about rotatable bonds.

Figures were generated using SYBYL 7.0 (Tripos Associates Inc., 1699 S Hanley Rd., St. Louis, MO 63144), PyMOL (DeLano, W. L., The PyMOL Molecular Graphics System (2002) DeLano Scientific, San Carlos, CA, http://www.pymol.org), Molscript,[25] BobScript,[26] and Raster3D.[27]

K_i Determinations. Both *wt* and K57A hPNMT were produced as described elsewhere.[6] A standard inhibition assay mixture contained 50 mM potassium phosphate pH 8.0 and 5 μM AdoMet (including [³H]-AdoMet) in a total volume of 250 μL. The concentration of phenylethanolamine was varied between $0.4-2.5 \times K_m$, while the inhibitor concentrations were varied between $0.4-2.5 \times K_i$. All 3-substituted inhibitors were used as the 3*R*-isomer, except **8**, which was racemic. Following the addition of enzyme, the reactions were incubated at 30 °C for 30 min and then quenched by the addition of 0.5 M boric acid (500 μL, pH 10.0). A total of 2 mL of a mixture of toluene/isoamyl alcohol (7:3) was added, and the samples were vortexed for 30 s. The phases were separated by centrifugation, and an aliquot of the organic phase (1 mL) was removed and added to 5 mL of scintillation fluid (Cytoscint, ICN). The radioactivity was quantitated by liquid scintillation spectrometry. Initial velocity data were then fitted to eq 1 using the Enzyme Kinetics module in SigmaPlot (SPSS Inc.).

$$v = \frac{V_{max}[S]}{[S] + K_m 1 + [I]/K_i} \tag{1}$$

In some cases, the value of K_i was similar to or lower than the enzyme concentration (4−10 nM) used in the assay. In those cases, the inhibitors were considered to be tight-binding,[28] and the data were fit to eq 2 using the competitive tight-binding inhibition routine in the Enzyme Kinetics module.

$$v = v_0 \frac{[E] - [I] - K_i^{app} + \sqrt{([E] - [I] - K_i^{app})^2 + 4[E]K_i^{app}}}{2[E]} \tag{2}$$

Here, v_0 and v are the reaction rates in the absence and presence of inhibitor, respectively, $[E]$ is the total enzyme concentration, $[I]$ is the inhibitor concentration, and K_i^{app} is the enzyme−inhibitor dissociation constant at a fixed concentration of substrate. The energies of interaction were calculated from K_i values using the Gibbs free energy eq 3

$$\Delta G = -RT(\ln K_i) \tag{3}$$

where R is the gas constant 1.9872 kcal/mol, T is the temperature of the experiment in degrees Kelvin (298 K), and K_i is the inhibition constant for the inhibitor.

Supporting Information Available: The electron density of each of the inhibitors. This material is available free of charge via the Internet at http://pubs.acs.org.

References

(1) Martin, J. L.; Begun, J.; McLeish, M. J.; Caine, J. M.; Grunewald, G. L. Getting the adrenaline going: Crystal structure of the adrenaline-synthesizing enzyme PNMT. *Structure* **2001**, *9*, 977−985.

(2) Grunewald, G. L.; Dahanukar, V. H.; Teoh, B.; Criscione, K. R. 3,7-Disubstituted-1,2,3,4-tetrahydroisoquinolines display remarkable potency and selectivity as inhibitors of phenylethanolamine *N*-methyltransferase versus the α_2-adrenoceptor. *J. Med. Chem.* **1999**, *42*, 1982−1990.

(3) Grunewald, G. L.; Seim, M. R.; Regier, R. C.; Martin, J. L.; Gee, C. L.; Drinkwater, N.; Criscione, K. R. Comparison of the binding of 3-fluoromethyl-7-sulfonyl-1,2,3,4-tetrahydroisoquinolines with their isosteric sulfonamides to the active site of phenylethanolamine *N*-methyltransferase. *J. Med. Chem.* **2006**, *49*, 5424−5433.

(4) McMillan, F. M.; Archbold, J.; McLeish, M. J.; Caine, J. M.; Criscione, K. R.; Grunewald, G. L.; Martin, J. L. Molecular recognition of sub-micromolar inhibitors by the epinephrine-synthesizing enzyme phenylethanolamine *N*-methyltransferase. *J. Med. Chem.* **2004**, *47*, 37−44.

(5) Gee, C. L.; Tyndall, J. D.; Grunewald, G. L.; Wu, Q.; McLeish, M. J.; Martin, J. L. Mode of binding of methyl acceptor substrates to the adrenaline-synthesizing enzyme phenylethanolamine *N*-methyltransferase: Implications for catalysis. *Biochemistry* **2005**, *44*, 16875−16885.

(6) Wu, Q.; Gee, C. L.; Lin, F.; Tyndall, J. D.; Martin, J. L.; Grunewald, G. L.; McLeish, M. J. Structural, mutagenic, and kinetic analysis of the binding of substrates and inhibitors of human phenylethanolamine *N*-methyltransferase. *J. Med. Chem.* **2005**, *48*, 7243−7252.

(7) Dunbrack, R. L., Jr.; Cohen, F. E. Bayesian statistical analysis of protein side-chain rotamer preferences. *Protein Sci.* **1997**, *6*, 1661−1681.

(8) Romero, F. A.; Vodonick, S. M.; Criscione, K. R.; McLeish, M. J.; Grunewald, G. L. Inhibitors of phenylethanolamine *N*-methyltransferase that are predicted to penetrate the blood−brain barrier: Design, synthesis and evaluation of 3-fluoromethyl-7-(*N*-substituted aminosulfonyl)-1,2,3,4-tetrahydroisoquinolines that possess low affinity toward the α_2-adrenoceptor. *J. Med. Chem.* **2004**, *47*, 4483−4493.

(9) Carosati, E.; Sciabola, S.; Cruciani, G. Hydrogen bonding interactions of covalently bonded fluorine atoms: From crystallographic data to a new angular function in the GRID force field. *J. Med. Chem.* **2004**, *47*, 5114−5125.

(10) Grunewald, G. L.; Romero, F. A.; Criscione, K. R. 3-Hydroxymethyl-7-(*N*-substituted aminosulfonyl)-1,2,3,4-tetrahydroisoquinoline inhibitors of phenylethanolamine *N*-methyltransferase that display remarkable potency and selectivity. *J. Med. Chem.* **2005**, *48*, 134−140.

(11) Grunewald, G. L.; Seim, M. R.; Lu, J.; Makboul, M.; Criscione, K. R. Application of the Goldilocks effect to the design of potent and selective inhibitors of phenylethanolamine *N*-methyltransferase: Balancing pK_a and steric effects in the optimization of 3-methyl-1,2,3,4-tetrahydroisoquinoline inhibitors by β-fluorination. *J. Med. Chem.* **2006**, *49*, 2939−2952.

(12) Najmanovich, R.; Kuttner, J.; Sobolev, V.; Edelman, M. Side-chain flexibility in proteins upon ligand binding. *Protein. Struct. Funct. Genet.* **2000**, *39*, 261−268.

(13) Teague, S. J. Implications of protein flexibility for drug discovery. *Nat. Rev. Drug Discovery* **2003**, *2*, 527−541.

(14) Pargellis, C.; Tong, L.; Churchill, L.; Cirillo, P. F.; Gilmore, T.; Graham, A. G.; Grob, P. M.; Hickey, E. R.; Moss, N.; Pav, S.; Regan, J. Inhibition of p38 MAP kinase by utilizing a novel allosteric binding site. *Nat. Struct. Biol.* **2002**, *9*, 268−272.

(15) Brünger, A. T.; Adams, P. D.; Clore, G. M.; Delano, W. L.; Gros, P.; Grosse-Kunstleve, R. W.; Jiang, J. S.; Kuszewski, J.; Nilges, N.; Pannu, N. S.; Read, R. J.; Rice, L. M.; Simonson, T.; Warren, G. L. Crystallography and NMR system (CNS): A new software system for macromolecular structure determination. *Acta Crystallogr., Sect. D: Biol. Crystallogr.* **1998**, *54*, 905−921.

(16) Jones, T. A.; Zou, J. Y.; Cowan, S. W.; Kjeldgaard, M. Improved methods for building protein models in electron density maps and the location of errors in these models. *Acta Crystallogr., Sect. A: Found. Crystallogr.* **1991**, *47*, 110−119.

(17) Emsley, P.; Cowtan, K. Coot: Model-building tools for molecular graphics. *Acta Crystallogr., Sect. D: Biol. Crystallogr.* **2004**, *60*, 2126−2132.

(18) Murshudov, G. N.; Vagin, A. A.; Dodson, E. J. Refinement of macromolecular structures by the maximum-likelihood method. *Acta Crystallogr., Sect. D: Biol. Crystallogr.* **1997**, *53*, 240−255.

(19) Schuettelkopf, A. W.; van Aalten, D. M. F. PRODRG−A tool for high-throughput crystallography of protein−ligand complexes. *Acta Crystallogr., Sect. D: Biol. Crystallogr.* **2004**, *60*, 1355−1363.

(20) Kleywegt, G. J.; Jones, T. A. Databases in protein crystallography. *Acta Crystallogr., Sect. D: Biol. Crystallogr.* **1998**, *54*, 1119−1131.

(21) Brünger, A. T. Free R value: A novel statistical quantity for assessing the accuracy of crystal structures. *Nature* **1992**, *355*, 672−475.

(22) Laskowski, R. A.; Macarthur, M. W.; Moss, D. S.; Thornton, J. M. Procheck−A program to check the stereochemical quality of protein structures. *J. Appl. Crystallogr.* **1993**, *26*, 283−291.

(23) Dundas, J.; Ouyang, Z.; Tseng, J.; Binkowski, A.; Turpaz, Y.; Liang, J. CASTp: Computed atlas of surface topography of proteins with structural and topographical mapping of functionally annotated residues. *Nucleic Acids Res.* **2006**, *34*, W116−W118.

(24) Lovell, S.; Word, J.; Richardson, J.; Richardson, D. The penultimate rotamer library. *Proteins* **2000**, *40*, 389−408.

(25) Kraulis, P. J. MOLSCRIPT: A program to produce both detailed and schematic plots of protein structures. *J. Appl. Crystallogr.* **1991**, *24*, 946−950.

(26) Esnouf, R. M. An extensively modified version of MolScript that includes greatly enhanced coloring capabilities. *J. Mol. Graphics Modell.* **1997**, *15*, 132−134, 112−113.

(27) Merritt, E. A.; Bacon, D. J. Raster3D photorealistic molecular graphics. *Methods Enzymol.* **1997**, *277*, 505−524.

(28) Wu, Q.; Criscione, K. R.; Grunewald, G. L.; McLeish, M. J. Phenylethanolamine *N*-methyltransferase inhibition: Re-evaluation of kinetic data. *Bioorg. Med. Chem. Lett.* **2004**, *14*, 4217−4220.